Multiplexed nanoplasmonic biosensor for one-step simultaneous detection of *Chlamydia trachomatis* and *Neisseria gonorrhoeae* in urine

Maria Soler[a], Alexander Belushkin[a], Andrea Cavallini[a], Carole Kebbi-Beghdadi[b], Gilbert Greub[b], Hatice Altug[a,*]

[a] *Institute of Bioengineering, École Polytechnique Fédérale de Lausanne (EPFL), Lausanne 1015, Switzerland*
[b] *Center for Research on Intracellular Bacteria (CRIB), Institute of Microbiology, University Hospital Center, University of Lausanne, Lausanne 1011, Switzerland*

ARTICLE INFO

ABSTRACT

Development of rapid and multiplexed diagnostic tools is a top priority to address the current epidemic problem of sexually transmitted diseases. Here we introduce a novel nanoplasmonic biosensor for simultaneous detection of the two most common bacterial infections: *Chlamydia trachomatis* and *Neisseria gonorrhoeae*. Our plasmonic microarray is composed of gold nanohole sensor arrays that exhibit the extraordinary optical transmission (EOT), providing highly sensitive analysis in a label-free configuration. The integration in a microfluidic system and the precise immobilization of specific antibodies on the individual sensor arrays allow for selective detection and quantification of the bacteria in real-time. We achieved outstanding sensitivities for direct immunoassay of urine samples, with a limit of detection of 300 colony forming units (CFU)/mL for *C. trachomatis* and 1500 CFU/mL for *N. gonorrhoeae*. The multiplexing capability of our biosensor was demonstrated by analyzing different urine samples spiked with either *C. trachomatis* or *N. gonorrhoeae*, and also containing both bacteria. We could successfully detect, identify and quantify the levels of the two bacteria in a one-step assay, without the need for DNA extraction or amplification techniques. This work opens up new possibilities for the implementation of point-of-care biosensors that enable fast, simple and efficient diagnosis of sexually transmitted infections.

1. Introduction

Sexually transmitted infections (STI) are one of the most common and widespread diseases around the world. Among them, infections caused by *Chlamydia trachomatis* (CT) and *Neisseria gonorrhoeae* (NG) stand out as the first and second more reported bacterial infections with nearly one million new cases each day (Newman et al., 2015). Though they are easily curable, most of the infections are asymptomatic and many individuals are not diagnosed and treated in a timely manner, which can lead to long-term sequelae like infertility, pelvic inflammatory disease, ectopic pregnancy or chronic pelvic pain (Newman et al., 2015). Current standard techniques for CT and NG detection rely on nucleic acid amplification tests (NAATs), which require laboratory settings and sample pretreatment procedures (e.g. cell lysis, DNA extraction) (Gaydos and Hardick, 2014; Mark et al., 2015; Papp et al., 2014). A rapid and simple detection of these pathogenic infections will not only facilitate a prompt treatment but also prevent onward transmission, help in risk awareness, reduce

economic expenses and significantly promote health care in resource-constrained environments.

Biosensors represent a unique opportunity to develop integrated systems that enable fast and accurate STI diagnosis. In particular, plasmonic technology offers label-free quantification, real-time analysis, high sensitivity and an extraordinary potential for miniaturization and integration in point-of-care devices (Brolo, 2012; Estevez et al., 2014). However, despite the powerful sensor technology and the progress made in integration, these next-generation biosensors still need to overcome important challenges to be greeted in the clinical field. For plasmonic biosensors working in label-free configuration, main limitations are related to the ability to detect multiple biomarkers simultaneously, with enough sensitivity, and directly in human fluids (Unser et al., 2015; Yoo and Lee, 2016). In the particular case of bacteria detection, a fully integrated biosensor capable of performing multiplexed and label-free detection at physiologically relevant concentrations has not been accomplished so far (Singh et al., 2014). Significant efforts are directed to improve the assay sensitivity by

---

performing sandwich immunoassays or employing magnetic beads for signal enhancement. With this methodology, one can reach limits of detection as low as 10–50 colony forming units (CFU)/mL (Sanvicens et al., 2011; Wang et al., 2012) or even 3 CFU/mL (Torun et al., 2012), but main drawbacks arise from the need of sample pretreatment or post-amplification steps. Others suggest the use of bacteriophages as recognition elements for direct analysis, achieving high sensitivities (10^1–10^3 CFU/mL) and also the possibility to evaluate antibiotic resistance (Tawil et al., 2013). Regarding multiplexed detection, Yoo et al. (2015) have developed a localized SPR sensor for high-throughput and simultaneous detection of different bacteria. Using aptamers as biorecognition elements they reached limits of detection around 10^4 CFU/mL in standard buffer conditions, but no tests in biological fluids or real samples were performed.

In this article, we present a novel nanoplasmonic biosensor for multiplexed detection of both *C. trachomatis* and *N. gonorrhoeae* directly in urine samples. Our biosensor is based on the extraordinary optical transmission (EOT) occurring in plasmonic nanohole arrays (Rodrigo et al., 2016). This sensing principle enables not only label-free and real-time detection but also the independent interrogation of each nanohole array simultaneously, which facilitates the high-throughput analysis in a simple manner. By selectively functionalizing the nanohole arrays with specific antibodies, we are able to capture and identify the bacteria present in urine samples and provide a rapid diagnosis without the need of cell lysis or DNA extraction. Furthermore, contrary to the conventional SPR based on the Kretschmann prism-coupling scheme, EOT can be achieved by normal light incidence and it is compatible with the use of light emitting diodes (LEDs) and CMOS (Complementary Metal Oxide Semiconductors) based imagers, allowing exceptional miniaturization and a wide field-of-view for multiplexing (Cetin et al., 2014; Chang et al., 2011). Therefore, the methodology we describe here represents a significant step forward for the implementation of a biosensor that enables a rapid, simple and efficient STI diagnosis.

2. Materials and methods

2.1. Materials and bacteria culture

The list of reagents and materials used in this work and details of nanofabrication, surface functionalization, and bacteria culture methods are provided in the Supplementary Information (SI).

2.2. Spectroscopic imaging and data processing

Plasmonic nanohole arrays (diameter 200 nm, period 600 nm) were fabricated via a lift-off-free wafer-scale fabrication scheme based on deep-UV lithography (details in the SI). For real-time biodetection experiments, we utilize an inverted microscope (Nikon Eclipse-Ti) and a CCD spectrometer (Andor Shamrock 303i). Briefly, a broadband light source illuminates the plasmonic microarray at normal incidence and the transmitted light is delivered to the spectrometer through a 400 μm width slit. For simultaneous analysis of 3 individual sensor arrays, we employ a 4× Nikon objective lens (NA=0.13) embedded in the microscope. The 3 sensors are aligned along the slit and each one is spread as a single spectrum via the grating (600 l/mm) inside the spectrometer. The wavelength range is adjusted to the EOT peak position (~850 nm) and spectra images are then recorded on a 1024×1024 CCD camera (iKon-M934) at 0.5 s of exposure time. Finally, the different spectra are independently extracted and analyzed with home-made MATLAB scripts to provide monitoring of the EOT peak shifting. The peak position is determined by calculating the centroid of the peak within a fixed wavelength window (40% maximum intensity) and plotted in real time. Sensorgrams show the centroid shifting *versus* time of the 3 independent sensor areas simultaneously.

2.3. Bacteria detection experiments

The biofunctionalized plasmonic chip is assembled with the microfluidics (details in SI) and connected to a syringe pump with adjustable pumping speed and a manually operated injection valve. Detection of bacteria is performed by injection of 200 μL of the samples over the biofunctionalized sensor surface at 20 μL/min flow rate. A continuous flow of acetate buffer (pH 5) is kept during the analysis. Signal increase was determined by extracting the difference in the mean of the centroid values (n≥100 data points) before the analyte capture and after rinsing. The antibody layer was regenerated (NaOH 20 mM) among measurements for optimization purposes. The same antibody layer could be used up to 10 detection cycles with a good reproducibility. Calibration curves are obtained by measuring different concentrations of bacteria in triplicate. Mean and standard deviation are plotted and fitted to a linear regression model. Limit of detection (LOD) is calculated as the concentration corresponding to the blank signal plus 3 times its standard deviation, while the limit of quantification (LOQ) is the concentration corresponding to the blank signal plus 10 times its standard deviation. Statistical analysis was performed as one-way analysis of variance (ANOVA) followed by Bonferroni's Multiple Comparison Test with statistical significance threshold set at 0.05 ($p < 0.05$). The data is analyzed using OriginPro 8.6 G software.

3. Results and discussion

3.1. Plasmonic nanohole array fabrication and microfluidics integration

In our biosensor, we employ a plasmonic chip composed of nanohole arrays fabricated on free-standing silicon nitride membranes. To create our plasmonic nanohole arrays we utilize a lift-off-free wafer-scale fabrication scheme based on deep ultra-violet (UV) lithography (Fig. 1a). Fabrication details are explained in the SI. Unlike the fabrication of plasmonic chips using electron beam lithography that requires sequential performance on each chip, our UV lithography-based procedure can be carried out at wafer scale providing thousands of plasmonic arrays with a high uniformity and reproducibility, and at low cost. This is extremely important in order to minimize the cost of the biosensor for an eventual implementation in point-of-care devices. Besides, our fabrication method is highly flexible so that plasmonic chips with multiple designs, incorporating different numbers of sensor areas, sizes, and spatial arrangements, can be easily created. For this work in particular, we employed a plasmonic microarray composed of 8 independent nanohole arrays (NHAs) separated with 1 mm distance and in a 3×3 matrix form. Each NHA has an area of 100×100 μm, with a hole diameter of 200 nm and 600 nm of array periodicity (Fig. 1b). The optical sensitivity of the plasmonic nanohole arrays was previously characterized achieving a bulk sensitivity around 600 nm/refractive index unit (RIU) (Cetin et al., 2014).

We integrated the plasmonic chip into a multichannel microfluidics system to facilitate sample delivery to the NHA sensor spots (Figs. 1c and d). The microfluidics was fabricated as a double-layer polydimethylsiloxane (PDMS) device by soft lithography employing specifically designed Si molds (details in the SI). The PDMS microfluidics contained 3 independent channels of 15 nL volume each (60 μm height, 500 μm width). Each channel included the 3 NHA sensors for multiplexed detection (Fig. 2) and it can be used individually for the analysis of different samples. The microfluidic setup allows for the use of low sample volumes and real-time monitoring of the bacteria capture. Furthermore, it reduces the human contact with the sample and simplifies the whole biosensor performance making it easier to operate.
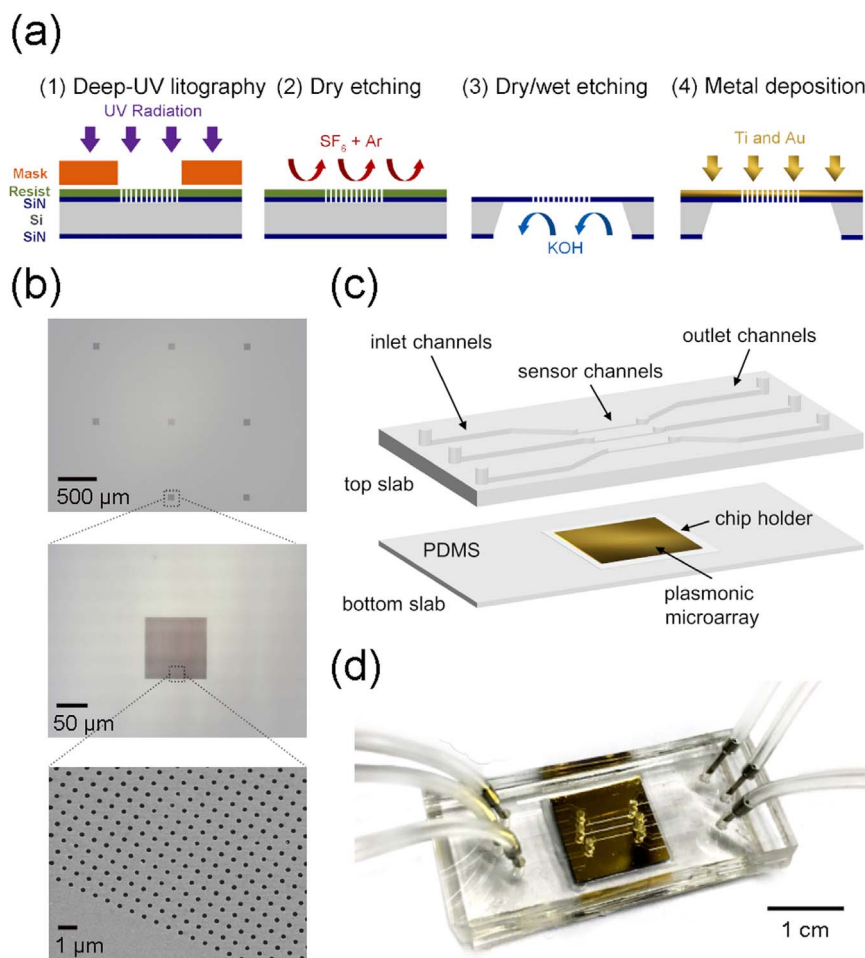
Fig. 1. Fabrication of plasmonic nanohole arrays and microfluidics integration: (a) Main fabrication steps of nanohole arrays on free-standing silicon nitride (SiN) membranes. (b) Optical microscope images of the plasmonic chip layout acquired with 4x objective (top) and 20× objective (middle). SEM image of a nanohole array (bottom). (c) Schematics of the microfluidics system. The top PDMS slab incorporates the 3 microfluidic channels with the inlet part, the sensor channels in contact with the plasmonic chip and the outlet part. The bottom PDMS slab serves as chip holder and facilitates the binding to the top layer. (d) Picture of the gold plasmonic chip assembled with the PDMS microfluidics and the tubing for sample delivery.

3.2. Multiplexed spectroscopic imaging in real time

For real-time and label-free biosensing, we utilize spectroscopic imaging based on the extraordinary optical transmission (EOT) phenomenon exhibited by the plasmonic nanohole arrays (Cetin et al., 2014). This exceptional enhancement of the light transmission is attributed to the grating coupling of an incident light with surface plasmon (SP) resonances and it is characterized by the appearance of a series of peaks and dips in the transmission spectrum. These SP modes are highly sensitive to minute changes in the near-field refractive index of the nanoholes, so they can be exploited for biosensing spectroscopy. When a biomolecular interaction takes place at the NHA surface, the variation of the refractive index induces a spectral shift in the EOT peak wavelength. Monitoring these spectral displacements enables the extraction of quantitative bioanalytical information in real time and in a label-free manner. The great sensing performance of our nano-plasmonic biosensor has been previously demonstrated for the detection of proteins and infectious viruses from biological media (Coskun et al., 2014; Yanik et al., 2010).

Fig. 2 shows a representative schematics of the biosensor platform and illustrative graphs describing the working principle. We illuminate the plasmonic microarray with a normally incident broadband light source and collect the transmitted light from 3 in-line NHAs simultaneously (Fig. 2a). In the spectrometer, the acquired CCD image is spread as individual spectra by using a medium grating (600 l/mm), showing the three EOT peaks corresponding to the three NHAs. In

aqueous solution, the EOT peak appears at 850 nm wavelength approximately (Fig. 2b). For measuring the peak displacements, we implemented a series of MATLAB scripts based on the centroid method. This data processing method consists in finding the center of mass of the curve over a certain wavelength window (i.e. centroid) and track it over time (Nenninger et al., 2002). We selected a wavelength window corresponding to the 40% of the intensity, including the maximum peak values plus the slopes. The slopes not only shift as much as the peak, but also show highly stable shape helping to reduce the spectral noise. Unlike using simple interrogation of the maximum peak value, with the centroid method we can extraordinarily minimize the noise coming from light instability or the spectrometer. This allows us to enhance the signal-to-noise ratio and achieve lower limits of detection. Furthermore, both centroid window determination and tracking of the spectra shifts (i.e. sensorgrams) were achieved using a user-friendly homemade interface, which allowed the real-time visualization of the binding events (Fig. 2c).

3.3. Chlamydia and gonorrhea bacteria capture and quantification

In order to detect the whole infectious bacteria directly from the urine without any sample processing, we employed antibodies as capturing probe. Even though immunoassays are presumably less sensitive than nucleic acid-based assays (Gaydos and Hardick, 2014), the later require a cell lysis pretreatment step that inevitably lengthens the analysis time. We selected specific antibodies against the major
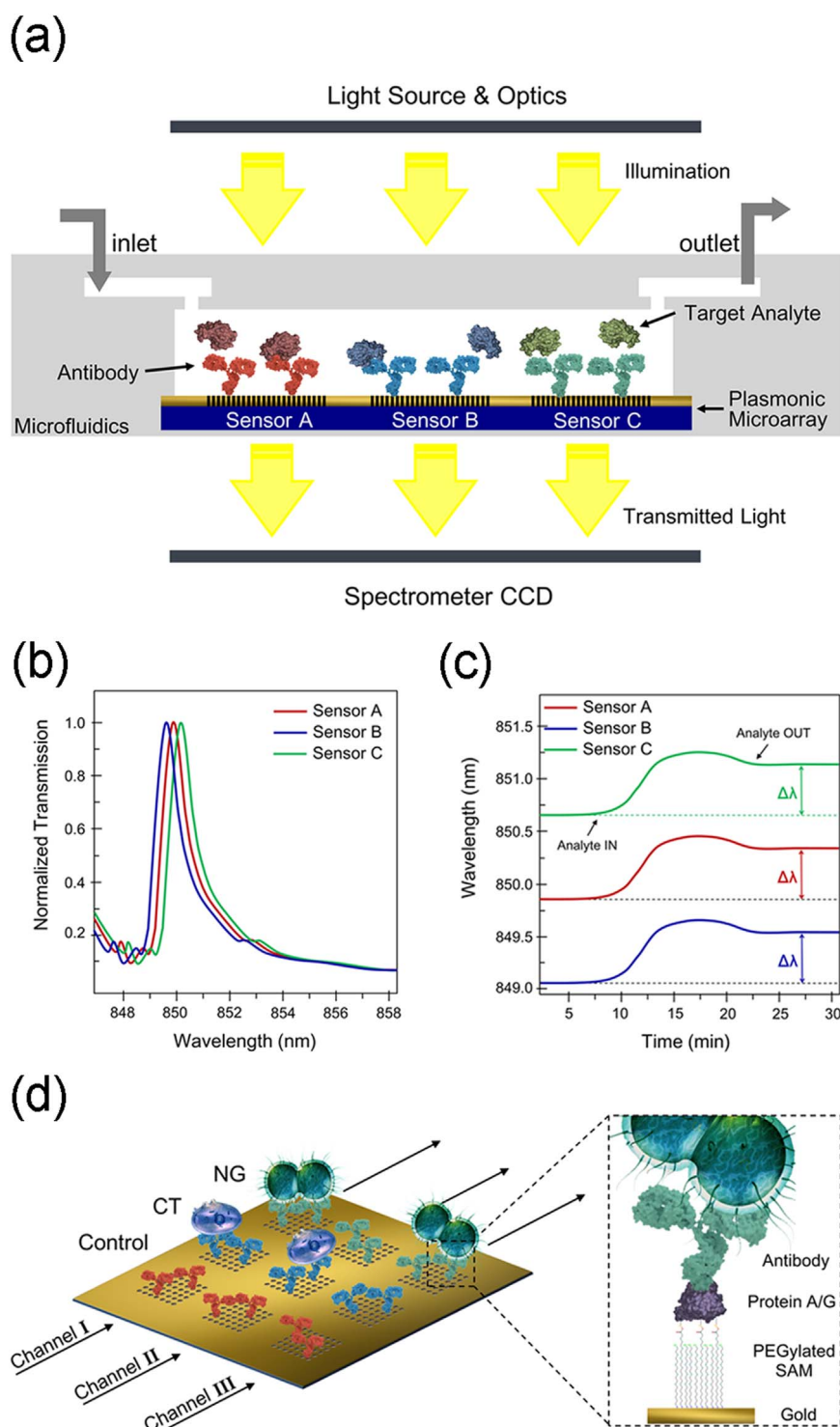
Fig. 2. Schematics of the nanoplasmonic biosensor working principle: (a) Cross-sectional overview of the biosensor set-up. (b) Representative graph illustrating the three EOT spectral peaks acquired simultaneously from the three sensor arrays (transmission *vs.* wavelength). (c) Representative graph illustrating the multiplexed real-time monitoring of the EOT wavelength shift (peak wavelength *vs.* time). (d) Schematics of the sensor surface biofunctionalization. The different nanohole arrays are modified with different antibodies: anti-Neisseria gonorrhoeae (NG) (green), anti-Chlamydia trachomatis (CT) (blue) and a control antibody (red). Each microfluidic channel (black arrows) covers 3 in-line sensor arrays so it includes the two specific sensors for the different bacteria plus the negative control sensor. The zoom-in section illustrates the surface chemistry strategy employed for the sensors functionalization.

outer membrane protein (MOMP) for both CT and NG bacteria. These antibodies present high affinity for the immunodominant antigen exposed on the outer part of the bacteria cell membranes, so they specifically recognize and capture the target specimen (Papp et al., 2014). In order to maximize the sensitivity of the assay and ensure the stability and robustness of the biorecognition layer, we applied a

functionalization strategy based on the protein A/G (Fig. 2d, details in SI). The protein A/G is a recombinant protein that presents high affinity for the Fc region of the antibodies, capturing them in an oriented manner and therefore guaranteeing available antigen binding sites (Kausaite-Minkstimiene et al., 2010; Makaraviciute et al., 2015; Mauriz et al., 2016; Sikkema, 1989). We immobilized the protein A/G

on the gold surface by covalently binding to a PEGylated self-assembled monolayer (SAM), which provides an antifouling and stable coating. For multiplexing purposes, antibody immobilization on the NHA was carried out employing a high-precision microdispenser, which permits the spotting of different antibody solutions on the different NHAs (100×100 µm) using less than 1 nL of sample (Fig. S4 in SI). In order to ensure the reliability and selectivity of our measurements, we defined one of the three in-line sensor arrays as our negative control reference, using the other two arrays for the specific capture of CT and NG respectively (Fig. 2d). We employed low concentrations of antibodies (10 µg/mL) to generate a sparse layer, which may reduce steric hindrance issues due to the big size of the bacteria. Finally, to get a robust and stable antibody layer we added a crosslinker (bis(sulfosuccinimidyl)suberate, BS3) which covalently binds the antibody to the protein A/G. This step is critical to avoid desorption of antibodies from the biosensor surface because of changes in the pH of the medium (Soler et al., 2014).

To evaluate the sensitivity and specificity of our biosensor for bacteria quantification we first focused on the detection of CT and NG individually in standard buffer conditions. For optimization purposes, in the laboratory we worked with purified and inactivated bacteria (details in SI). We selected an inactivation procedure (i.e. 10% formalin) that preserves the outer membrane structure of the bacteria intact (Chao and Zhang, 2011), hence the capture with MOMP antibodies is still possible and it is analogue to employing live bacteria cells. Acetate buffer at pH=5 was selected as our standard buffer to minimize electrostatic repulsion between the bacteria and our functionalized surface (details in SI). We obtained both standard calibration curves (Fig. 3) by introducing CT and NG spiked samples covering a wide range of concentrations, from 10 to 10^7 CFU/mL (10-fold dilution). Signals were collected from the NHA sensors previously functionalized with anti-CT and anti-NG antibodies, respectively. We observed increasing wavelength shifts in a concentration-dependent manner (Fig. S6 in SI), directly correlated with the interaction between the bacteria and its corresponding antibody. Furthermore, to demonstrate the selectivity of our biosensor we also tested the possible binding of the bacteria to the unspecific antibodies. We flowed NG samples over the anti-CT antibody, and vice versa (Fig. 3). Even when using large concentrations of bacteria, nonspecific signals were negligible. This corroborates that the wavelength shifts obtained for the standard calibration curves exclusively came from specific capture of the specific bacteria, verifying the accuracy of our label-free quantification. By fitting the data to a linear regression model (R^2(CT)=0.98, R^2(NG)=0.99) we could determine the Limit of Detection (LOD) and Limit of Quantification (LOQ) of our biosensor, defined as the concentration corresponding to the blank signal plus 3 times or 10 times its standard deviation, respectively (Eurachem, 1998). We achieved a LOD of 400 CFU/mL for CT and 1000 CFU/mL for NG. The limits of quantification (LOQ) were found at 760 CFU/mL for CT and 2800 CFU/mL for NG. These detection limits were considered greatly satisfactory for diagnosis since they cover the physiological concentration range found in the majority of the infection cases (Jaton et al., 2006). Moreover, these results prove the high sensitivity of our nanoplasmonic biosensor compared to the state-of-the-art technology. The use of plasmonic biosensors for direct and label-free detection of pathogenic microorganisms in human fluids (e.g. SPR or localized SPR platforms) has been limited so far by the low sensitivity of the assays, usually reporting LODs in the range of 10^4 to 10^7 CFU/mL (Ahmed et al., 2014; Huang et al., 2014; Tokel et al., 2015; Yoo and Lee, 2016). With our biosensor, we reached more than 10 times lower detection limit ($< 10^3$ CFU/mL).

In addition, we evaluated the repeatability and accuracy of our measurements by determining the inter-assay coefficients of variation (i.e. variability between assays performed with different plasmonic chips) for the quantification of both bacteria (Table S1 in SI). The values for the inter-assay CV were below 15% in all cases, which is the
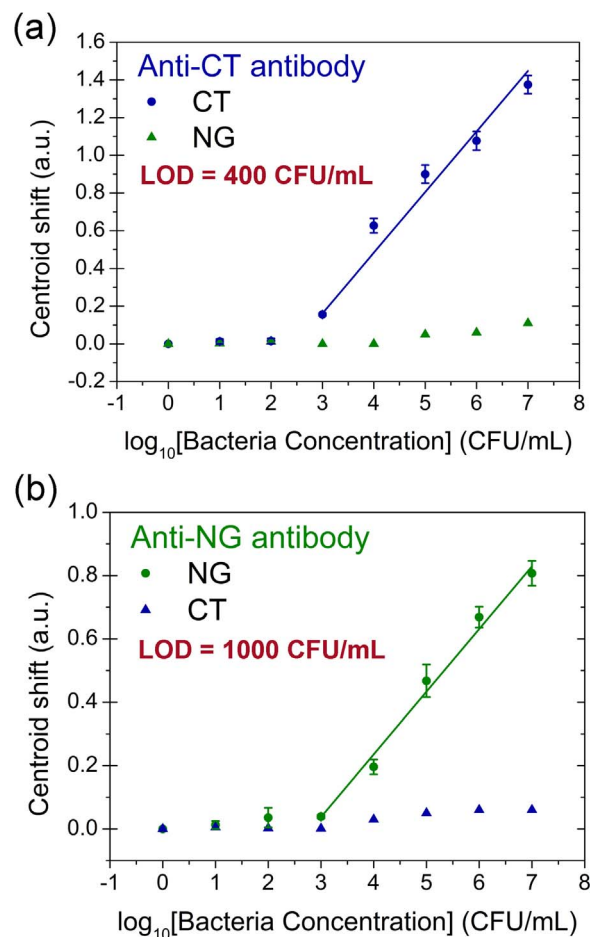

Fig. 3. Evaluation of the sensitivity and selectivity for the detection and quantification of both bacteria in buffer. (a) Standard calibration for specific detection of Chlamydia trachomatis (CT) (blue). Signals are obtained by flowing CT samples at different concentrations (10^1–10^7 CFU/mL) over a sensor array functionalized with anti-CT antibody. Green triangles represent nonspecific binding of Neisseria gonorrhoeae (NG) on the anti-CT antibody array. (b) Standard calibration for specific detection of NG (green). Signals are obtained by flowing NG samples at different concentrations (10^1–10^7 CFU/mL) over a sensor array functionalized with anti-NG antibody. Blue triangles represent nonspecific binding of CT on the anti-NG antibody array. Each data point represents the mean and standard deviation of three replicates. Data is fitted to a linear regression model.

maximum variability recommended for clinical analysis. This demonstrates the reproducibility of the assay and proves the robustness of the methodology. Finally, to further validate the bacteria capture on the nanohole arrays we performed post-experiment SEM imaging of the chips (Fig. S7 in SI). The images showed both specific bacteria captured on the nanohole arrays, so we can confirm that sensor responses came from direct detection of the pathogens.

3.4. Direct detection of chlamydia and gonorrhea in urine

To validate the potential of our biosensor for its clinical application we addressed the direct measurement in urine samples. This is essential to offer a fast diagnosis of STI that does not require any sample pretreatment to be performed in clinical laboratories. Moreover, the selection of urine as the biological sample permits a simple and non-invasive analysis that could be eventually carried out at different points of care, such as doctor's office, planned parenthood care centers or even directly by the user at home. One of the main limitations for urine analysis is the extreme variability of the composition. Several parameters like the concentration of certain proteins vary over a wide range between different subjects, the diet or the collection
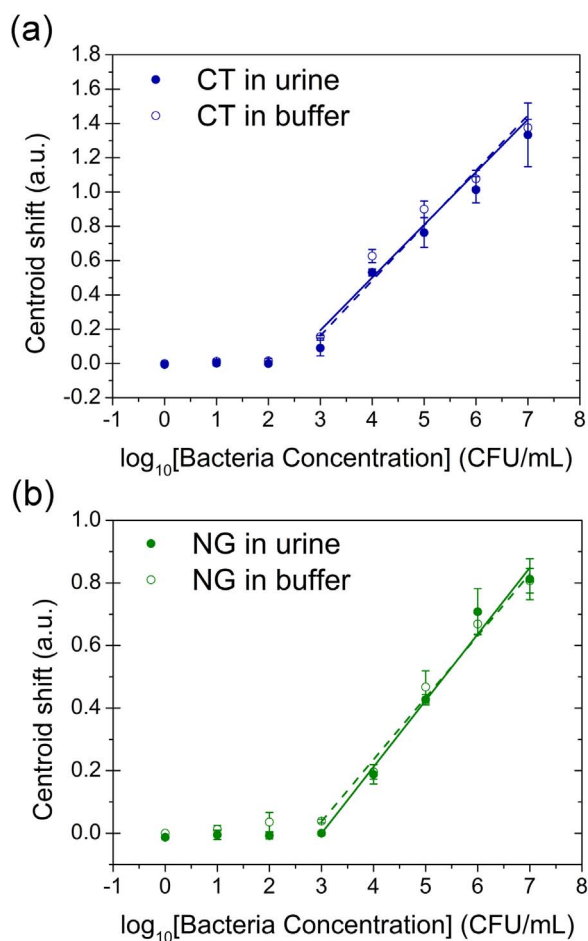
Fig. 4. Quantification of bacteria in urine and comparison to standard buffer samples. (a) Standard calibration for CT in urine (solid line) and in buffer (dashed line). Signals are obtained by flowing urine or buffer samples spiked with different concentrations of CT over a sensor array functionalized with anti-CT antibody. (b) Standard calibration for NG spiked in urine (solid line) and in buffer (dashed line). Signals are obtained by flowing urine or buffer samples spiked with different concentrations of NG over a sensor array functionalized with anti-NG antibody. Each data point represents the mean and standard deviation of three replicates. Data is fitted to a linear regression model.

time (Rose et al., 2015). This variability in composition can result in a higher or lower background that we should take into account when extracting our specific signal (Soler et al., 2016). Therefore, the presence of a control sensor in the same microfluidic channel becomes indispensable to ensure the reliability of the assay. The multiplexing design of our biosensor allows us to bring every single sample simultaneously in contact with the sensor arrays functionalized with different antibodies, including a nonspecific common mouse antibody that provides the negative control. Signals acquired from this control sensor represent the background response corresponding to the nonspecific adsorption of matrix components (e.g. proteins), thereby providing a precise reference for the subtraction of the specific signal (details in SI).

In this way, we obtained both calibration curves for the detection of CT and NG in urine. Different concentrations of CT and NG (from 10 to 10^7 CFU/mL) were spiked in negative urine samples and flowed over the functionalized NHAs. Urine was employed directly as obtained, without performing any purification or filtration treatment. The sensor response obtained from negative urine samples was considered our blank signal in this case. Fig. 4 shows the detection curves for the two bacteria when plotting the specific signal after subtracting the reference background. We compared the obtained calibration curves in urine to the standard calibration performed in buffer. As can be seen, the curves for both conditions (i.e. urine and buffer) appear identical. This

confirms that matrix components present in the urine do not influence the bacteria capture and also that the sensor signal obtained after reference subtraction solely comes from specific CT or NG detection. Analytical sensitivity was also determined for measurements in urine by calculating both limits of detection and quantification. For CT detection, the LOD was 300 CFU/mL and the LOQ was 590 CFU/mL. For NG detection, the LOD was 150 CFU/mL and the LOQ was 3900 CFU/mL. These values are comparable to the ones obtained in buffer conditions, therefore, validating the reliability of our methodology.

3.5. Multiplexed analysis of chlamydia and gonorrhea in urine samples

Finally, we proved the multiplexing capabilities of our nanoplasmonic biosensor for simultaneous detection of both STI bacteria. The microarray chip was functionalized with the three different antibodies (anti-CT, anti-NG and control) and assembled with the microfluidics in such a way that each channel included the 3 different sensors. Signals were collected from the three individual NHAs at the same time. In a first experiment, we introduced a negative urine sample obtained from a healthy donor (Fig. 5a). The exact same response was acquired from the 3 independent sensor arrays. Since the healthy urine sample did not contain any bacteria sample, we can attribute the response to the nonspecific binding of protein components of the urine to the sensor surface. This also confirmed that the background signal is equivalent for the 3 sensors, so the reference subtraction method is accurate. Next, we introduced a urine sample spiked with CT at 10^7 CFU/mL (Fig. 5b). We could observe a high positive signal coming from the anti-CT functionalized sensor (blue line), while there is no cross-reactivity with the anti-NG functionalized sensor (green line). In a third experiment, we introduced a urine sample spiked with NG at the same concentration (10^7 CFU/mL) (Fig. 5c). In this case, the specific detection signal only arises from the specific anti-NG functionalized sensor (green line), with an insignificant cross-reactivity coming from the anti-CT functionalized sensor (blue line). In addition, we performed a fourth experiment by introducing a urine sample spiked with both CT and NG bacteria at 10^7 CFU/mL (Fig. 5d). As we expected, the sensorgram showed positive signals coming from both anti-CT and anti-NG functionalized sensors but no signal in the negative control, which remained at the background level. Statistical analysis confirmed that there were no significant differences between the signals obtained when measuring each bacteria sample separately (Figs. 5b and c) or both bacteria coexisting in the same sample (Fig. 5d) (n_{CT}=4, p > 0.05; n_{NG}=4, p_{NG} > 0.05). Moreover, the signals measured in this multiplexed configuration also matched with the signals obtained when measuring each bacteria individually (Fig. 4). This demonstrates that we were able to selectively capture, identify and quantify both CT and NG simultaneously in a single urine sample.

We have demonstrated that our nanoplasmonic microarray allows for multiplexed and label-free detection of STI bacteria with no cross-reactivity. The proposed methodology has proved to be reliable and accurate for the direct detection of whole-cell bacteria in urine samples, without requiring any sample pretreatment or amplification. Furthermore, our technology is easily scalable to further include a large number of sensor arrays for truly high-throughput analysis. In this regard, on-going work is dedicated to the study and validation of clinical samples and possible incorporation of other biomarkers that ensure the diagnosis sensitivity and specificity. This, together with integration in a handheld point-of-care device would permit a simple identification and diagnosis of STI in few minutes and using only a few microliters of urine.

4. Conclusions

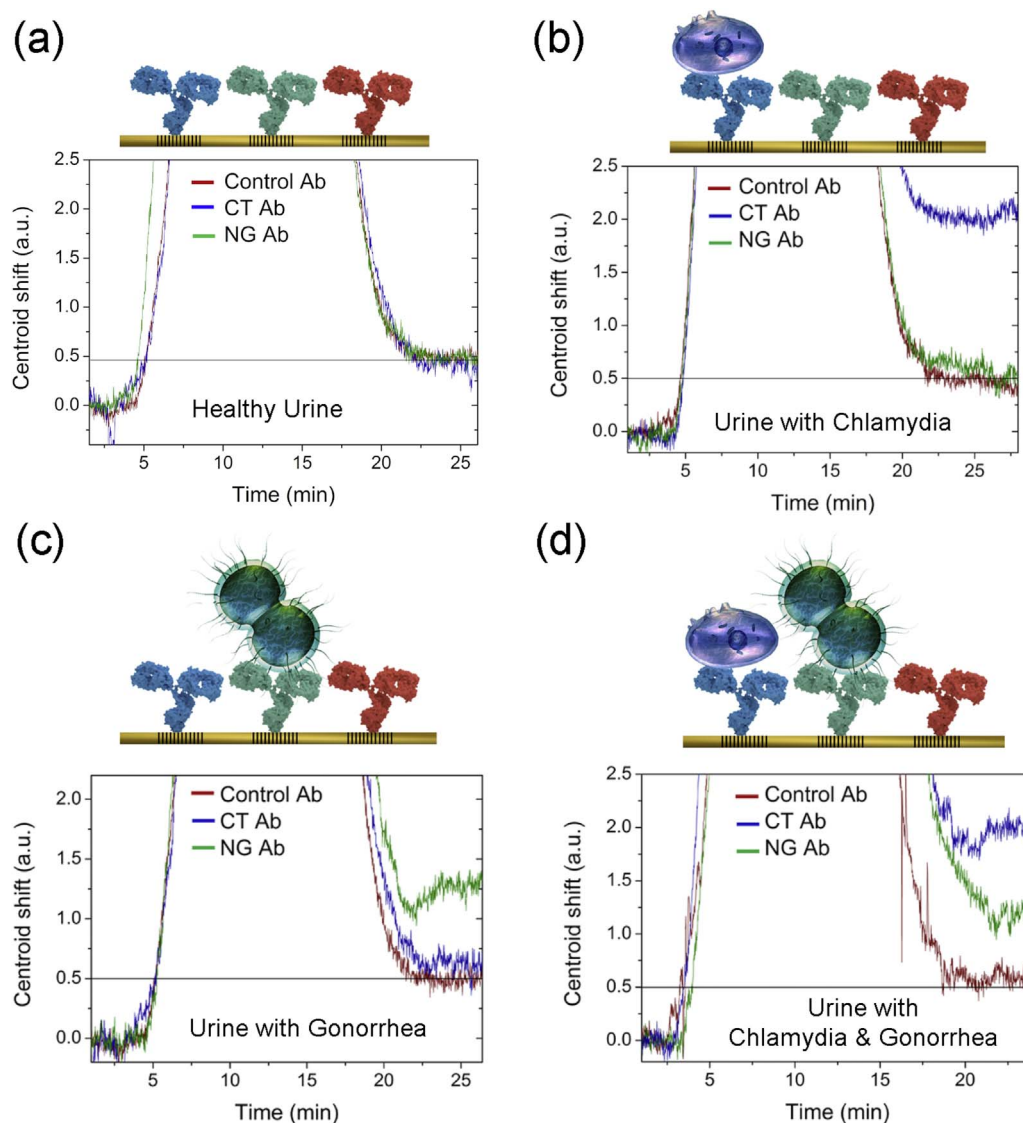We have developed a novel nanoplasmonic biosensor for simulta-

Fig. 5. Multiplexed analysis of different bacteria in urine. Sensorgrams show the signals corresponding to the three arrays functionalized with anti-CT antibody (blue), anti-NG antibody (green) and the control antibody (red). Horizontal black line serves as reference to identify the urine background signal. (a) Background signal from negative a healthy urine sample. (b) Specific detection of a CT spiked sample (10^7 CFU/mL) (blue line). (c) Specific detection of a NG spiked sample (10^7 CFU/mL) (green line). (d) Detection of both CT and NG spiked in the same sample (10^7 CFU/mL each) (blue and green line).

neous diagnosis of *C. trachomatis* and *N. gonorrhoeae* infections in urine. Our plasmonic microarray based on gold nanohole sensors offers highly sensitive, label-free and multiplexed analysis in real time. Microfluidic integration and a thorough optimization of surface biofunctionalization provided a direct and fast quantification of CT and NG bacteria with excellent selectivity, accuracy and proved reliability and robustness. We have achieved outstanding detection sensitivities measuring directly in urine samples, without the need of DNA extraction or post-amplification steps. We have also demonstrated the ability of our nanoplasmonic microarray for truly multiplexed detection of different bacteria in a one-step assay. To our knowledge, this is the first report showing label-free and multiplexed nanoplasmonic sensing of bacteria directly in biological samples and within a physiologically relevant concentration without the need for amplification steps.

The work presented in this article represents a decisive and necessary step towards the implementation of point-of-care diagnostics. Our biosensor can be easily integrated into a portable handheld device employing LED sources and CMOS detector, which significantly reduces the costs and enables the analysis performance outside the

clinical laboratory. Furthermore, the direct detection of the bacteria in urine samples can provide a "while-you-wait" diagnosis of STI in a noninvasive manner. This definitely signifies a breakthrough in the field of sexually transmitted diseases, not only for diagnosis but for transmission prevention and early treatment.

Appendix A. Supporting information

Supplementary data associated with this article can be found in the online version at doi:10.1016/j.bios.2017.03.047.

References

Ahmed, A., Rushworth, J.V., Hirst, N.A., Millner, P.A., 2014. Clin. Microbiol. Rev. 27 (3), 631–646.

Brolo, A.G., 2012. Nat. Photonics 6 (11), 709–713.

Cetin, A.E., Coskun, A.F., Galarreta, B.C., Huang, M., Herman, D., Ozcan, A., Altug, H., 2014. Light Sci. Appl 3 (1), e122.

Chang, T.-Y., Huang, M., Yanik, A.A., Tsai, H.-Y., Shi, P., Aksu, S., Yanik, M.F., Altug, H., 2011. Lab a Chip 11 (21), 3596–3602.

Chao, Y., Zhang, T., 2011. Appl. Microbiol. Biotechnol. 92 (2), 381–392.

Coskun, A.F., Cetin, A.E., Galarreta, B.C., Alvarez, D.A., Altug, H., Ozcan, A., 2014. Sci. Rep. 4, 6789.

Estevez, M.-C., Otte, M.A., Sepulveda, B., Lechuga, L.M., 2014. Anal. Chim. Acta 806, 55–73.

Eurachem, 1998. Lab. Gov. Chem..

Gaydos, C., Hardick, J., 2014. Expert Rev. Anti Infect. Ther. 12 (6), 657–672.

Huang, C.J., Knoll, W., Sessitsch, A., Dostalek, J., 2014. Talanta 122, 166–171.

Jaton, K., Bille, J., Greub, G., 2006. J. Med. Microbiol. 55 (12), 1667–1674.

Kausaite-Minkstimiene, A., Ramanaviciene, A., Kirlyte, J., Ramanavicius, A., 2010. Anal. Chem. 82 (15), 6401–6408.

Makaraviciute, A., Ramanavicius, A., Ramanaviciene, A., 2015. Anal. Methods 7 (23), 9875–9884.

Mark, H., Dhir, A., Roth, C., 2015. Am. J. Nurs. 115 (9), 34–44.

Mauriz, E., García-Fernández, M., Lechuga, L., 2016. Trends Anal. Chem. 79, 191–198.

Nenninger, G.G., Piliarik, M., Homola, J., 2002. Meas. Sci. Technol. 13 (12), 2038.

Newman, L., Rowley, J., Vander Hoorn, S., Wijesooriya, N.S., Unemo, M., Low, N., Stevens, G., Gottlieb, S., Kiarie, J., Temmerman, M., 2015. PloS One 10 (12), e0143304.

Papp, J.R., Schachter, J., Gaydos, C.A., Van Der Pol, B., 2014. Recomm. Rep. CDC 63, 1.

Rodrigo, S.G., de León-Pérez, F., Martín-Moreno, L., 2016. Proceedings of the IEEE.

Rose, C., Parker, A., Jefferson, B., Cartmell, E., 2015. Crit. Rev. Environ. Sci. Technol. 45 (17), 1827–1879.

Sanvicens, N., Pascual, N., Fernández-Argüelles, M.T., Adrián, J., Costa-Fernández, J.M., Sánchez-Baeza, F., Sanz-Medel, A., Marco, M.-P., 2011. Anal. Bioanal. Chem. 399 (8), 2755–2762.

Sikkema, W.D., 1989. Am. Biotechnol. Lab 7 (4 A), (42-42).

Singh, R., Mukherjee, M.D., Sumana, G., Gupta, R.K., Sood, S., Malhotra, B., 2014. Sens Actuators B Chem. 197, 385–404.

Soler, M., Estevez, M.-C., de Lourdes Moreno, M., Cebolla, A., Lechuga, L.M., 2016. Biosens. Bioelectron. 79, 158–164.

Soler, M., Estevez, M., Alvarez, M., Otte, M.A., Sepulveda, B., Lechuga, L.M., 2014. Sensors 14 (2), 2239–2258.

Tawil, N., Mouawad, F., Lévesque, S., Sacher, E., Mandeville, R., Meunier, M., 2013. Biosens. Bioelectron. 49, 334–340.

Tokel, O., Yildiz, U.H., Inci, F., Durmus, N.G., Ekiz, O.O., Turker, B., Cetin, C., Rao, S., Sridhar, K., Natarajan, N., 2015. Sci. Rep. 5, 9152.

Torun, Ö., Boyacı, İ.H., Temür, E., Tamer, U., 2012. Biosens. Bioelectron. 37 (1), 53–60.

Unser, S., Bruzas, I., He, J., Sagle, L., 2015. Sensors 15 (7), 15684–15716.

Wang, Y., Knoll, W., Dostalek, J., 2012. Anal. Chem. 84 (19), 8345–8350.

Yanik, A.A., Huang, M., Kamohara, O., Artar, A., Geisbert, T.W., Connor, J.H., Altug, H., 2010. Nano Lett. 10 (12), 4962–4969.

Yoo, S.M., Kim, D.-K., Lee, S.Y., 2015. Talanta 132, 112–117.

Yoo, S.M., Lee, S.Y., 2016. Trends Biotechnol. 34 (1), 7–25.